Lambda-PFLOTRAN 1.0: Workflow for Incorporating Organic Matter Chemistry Informed by Ultra High Resolution Mass Spectrometry into Biogeochemical Modeling

Katherine A. Muller[1], Peishi Jiang[1], Glenn Hammond[1], Tasneem Ahmadullah[1], Hyun-Seob Song[2], Ravi Kukkadapu[1], Nicholas Ward[3], Madison Bowe[3], Rosalie K. Chu[1], Qian Zhao[1], Vanessa A. Garayburu-Caruso[1], Alan Roebuck[3], Xingyuan Chen[1]

[1] Pacific Northwest National Laboratory, Richland, WA 99352, USA
[2] Department of Biological Systems Engineering, University of Nebraska—Lincoln, Lincoln, Nebraska, USA
[3] Pacific Northwest National Laboratory, Sequim WA 98382, USA

Correspondence to: Katherine Muller (katherine.muller@pnnl.gov)

For submission to Geoscientific Model Development

Abstract. Organic matter (OM) composition plays a central role in microbial respiration of dissolved organic matter and subsequent biogeochemical reactions. Here, a direct connection of organic matter chemistry and thermodynamics to reactive transport simulators has been achieved through the newly developed Lambda-PFLOTRAN workflow tool that succinctly incorporates carbon chemistry data generated from Fourier transform ion cyclotron resonance mass spectrometry (FTICR-MS) into reaction networks to simulate organic matter degradation and the resulting biogeochemistry. Lambda-PFLOTRAN is a python-based workflow, executed through a Jupyter Notebook interface, that digests raw FTICR-MS data, develops a representative reaction network based on substrate-explicit thermodynamic modeling (also termed lambda modeling due to its key thermodynamic parameter λ used therein), and completes a biogeochemical simulation with the open source, reactive flow and transport code PFLOTRAN. The workflow consists of the following five steps: configuration, thermodynamic (lambda) analysis, sensitivity analysis, parameter estimation, and simulation output and visualization. Two test cases are provided to demonstrate the functionality of the Lambda-PFLOTRAN workflow. The first test case uses laboratory incubation data of temporal oxygen depletion to fit lambda parameters (i.e., maximum utilization rate and microbial carrying capacity). A slightly more complex second test case fits multiple lambda formulation and soil organic matter release parameters to temporal greenhouse gas generation measured during a soil incubation. Overall, the Lambda-PFLOTRAN workflow facilitates upscaling by using molecular-scale characterization to inform biogeochemical processes occurring at larger scales.

1 Introduction

Microbial respiration of dissolved organic carbon (DOC) is a main driver of environmental biogeochemical processes. Mechanistic biogeochemical models often rely on lumping organic matter into a few distinct carbon pools (e.g., dissolved, sorbed, mineral associated or refractory, labile, etc.) (e.g., Fatichi, et al., 2019, Robertson et al., 2019, Wang et al., 2013) but do not fully consider the properties of the organic matter (OM) compounds individually. Pooled carbon approaches have benefits, such as assigning variable levels of bioavailability, however, this approach does not capture the complex temporal dynamics of respiration driven by OM composition, as aerobic respiration rates have been linked to organic carbon concentration, thermodynamics of the OM (Stegen et al., 2018, Garayburu-Caruso et al., 2020), as well as the diversity of OM compounds present (Lehmann et al. 2020, Stegen et al., 2022). Such findings highlight the importance of incorporating individual OM chemistry into biogeochemical modeling to capture, and ultimately predict, system behavior more accurately.

There are many advanced instrumentation techniques capable of detecting and identifying individual OM formulae that comprise a bulk OM sample (e.g., GC-MS, HPLC-MS, Fourier transform ion cyclotron resonance mass spectrometry [FTICR-MS], etc.). For instance, FTICR-MS is a powerful, high-resolution, method that identifies molecular formulae for individual organic compounds. In any given environmental sample, FTICR-MS (or other ultra high-resolution methods) will typically resolve thousands of discrete OM molecular formulae, each with a unique mass and elemental composition (Cooper et al., 2020, Bahureksa et al., 2021). However, untargeted analytical techniques like FTICR-MS are only able to determine if a compound is present and cannot quantify the total concentration associated with each organic matter molecule. Still, such techniques do provide immense amounts of characterization data encompassing a deeper analytical window than measuring a small number of individual biomarkers quantitatively (e.g., Ward et al., 2013). Utilizing such high-resolution molecular data in reactive transport modeling frameworks affords new opportunity to advance carbon cycling in terrestrial, riverine and coastal systems despite of various theoretical and computational challenges.

Substrate-explicit thermodynamic modeling (SXTM) provides an avenue for incorporating individual OM reactivity based on thermodynamics (Song et al., 2020) into reactive transport models. The SXTM procedure takes the individual chemical formula derived from FTICR-MS (or another high-resolution technique) and uses its thermodynamic properties to generate an oxidation reaction for each molecular formula present in a sample. The corresponding reaction stoichiometry is then determined by considering catabolic, anabolic, and metabolic reactions and balancing energy for the overall metabolic reaction, allowing for the development of an aerobic respiration expression for each OM formula.

Still, the sheer number of compounds identified in each sample proves difficult for model integration. Typically, reactive transport simulators consider only a small number of primary species in their reaction networks, and most could not support modeling each of the thousands of organic matter molecules individually. Here, the developed Lambda-PFLOTRAN workflow addresses this challenge through grouping, or binning, similar compounds based on

64   their thermodynamic properties, allowing for the number of species considered within the reaction network to be

65   reduced, and thus decreasing the required computational resources.

66   Lambda-PFLOTRAN is a python-based workflow that digests raw FTICR-MS data, develops a representative reaction

67   network based on substrate-explicit thermodynamic modeling (Song et al., 2020), and completes a biogeochemical

68   simulation with the open source, parallel reactive flow and transport code, PFLOTRAN (Hammond et al., 2014).

69   PFLOTRAN is developed under an open source, GNU LGPL license. The term 'lambda' is used here because λ is a

70   key parameter in the SXTM, which quantifies thermodynamic favorability of aerobic respiration of OM. The

71   connection between the unique reaction network developed for each FTICR-MS sample hinges on the use of

72   PFLOTRAN's reaction sandbox capability (Hammond, 2022). The reaction sandbox gives the ability to define

73   additional custom, kinetic reactions beyond standard formulations (e.g., mineral precipitation-dissolution, Michaelis-

74   Menten, etc.). The Lambda-PFLOTRAN workflow enables upscaling by using molecular-scale information to inform

75   larger scale biogeochemical processes occurring throughout a watershed which can be simulated with PFLOTRAN.

76   Herein we describe the Lambda-PFLOTRAN workflow process including the governing expressions, workflow steps,

77   data requirements, as well as the associated assumptions and limitations. Two illustrative test cases are also included

78   to demonstrate the workflow.

79   **2 Methods**

80   **2.1 Conceptual Model**

81   Respiration modeling herein is based on thermodynamic theory by Desmond-Le Quemener and Bouchez (2014) which

82   was updated for multiple OM formulas by Song et al. (2020). The generalized form of OM molecule is assumed to

83   take the form of $C_aH_bN_cO_dP_eS^{z}_f$. Each molecular formula then undergoes respiration (i.e., reaction with oxygen) based

84   on the following general reaction expression:

85    $y_{OM_i}OM_i + y_{H_2O}H_2O + y_{HCO_3}{}^-HCO_3{}^- + y_{NH_4}{}^+NH_4{}^+ + y_{HPO_4}{}^{--}HPO_4{}^{--} + y_{HS}{}^-HS^- + y_{H}{}^+H^+ + y_{e}{}^-e^- +$

86    $y_{O_2}O_2 + y_BBM = 0,$ $\hspace{3cm} (1)$
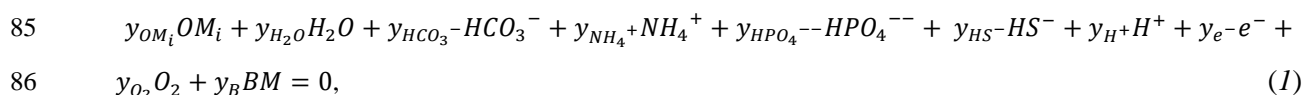
87   This generalized expression is used to describe the oxidation of any OM molecule, *i,* and has been normalized to one

88   mole of biomass (BM) produced. BM is assumed to have a formula of $CH_{1.8}O_{0.5}N_{0.2}$ (Stephanopoulos et al.,

89   1998; Kleerebezem and Van Loosdrecht, 2010). OM_i represents the OM molecules as informed by FTICR-MS. Each

90   *y* represents the reaction stoichiometry for that reactant ($y < 0$) or product ($y > 0$). While this expression is specific for

91   cases where oxygen is the electron acceptor, such an expression could be updated for alternative electron acceptors.

92   Substrate-explicit thermodynamic modeling expressions developed from Song et al. (2020) were implemented in a

93   reaction sandbox within PFLOTRAN. The expressions were implemented in a general manner allowing for flexibility

94   in handling variations in FTICR-MS data and several user adjustable analysis configurations.

95   The microbial growth kinetics are described by Eq. (2):

96      $\mu_i{}^{kin} = \mu^{max}exp(-\frac{\alpha|y_{OM,i}|}{1000V_h[OM,i]})exp(-\frac{\alpha|y_{O_2,i}|}{1000V_h[O_2]})$,   (2)

97   where $\mu_i{}^{kin}$ is the unregulated uptake rate of reaction for OM_i [hr^{-1}], μ^{max} is the maximal microbial growth rate [hr^{-1}

98   ], $y_{OM,i}$ is the stoichiometry for OM_i [mol-OM · mol-biomass^{-1}], V_h is microbial harvest volume [m^3]. Given the

99   physical interpretation of V_h as the microbial harvest volume, it is assumed here that the value of V_h is the same for

100   both OM_i and O_2, [OM_i] is the organic matter concentration of OM_i [mol-OM·L^{-1}], $y_{O_2,i}$ is the stoichiometry for O_2

101   for respiration of OM_i [mol-O_2·mol-biomass^{-1}], [O_2] is oxygen concentration [mol-O_2·L^{-1}], α is a microbial unit

102   conversion [mol-biomass] and 1000 is the conversion of m^3 to L.

103   Further, using a cybernetic modeling approach (after Song et al., 2018), all the unregulated uptake rates ($\mu_i{}^{kin}$) are

104   normalized by the sum of unregulated uptake rates across all reactions, i following Eq. (3):

105      $u_i = \frac{\mu_i{}^{kin}}{\sum_{i=1}^{n}\mu_i{}^{kin}}$ (3)

106   where u_i is the fraction of the unregulated rate [-]. The final regulated rate, r_i [hr^{-1}] for each reaction is then computed

107   following Eq. (4):

108      $r_i = u_i\mu_i{}^{kin}$,   (4)

109   For implementation within PFLOTRAN, the use of inhibition terms was required to prevent negative concentrations

110   once a reactant is nearly depleted. For a reaction to proceed, all reactant species must be present above a minimum

111   concentration even if the molecules do not explicitly control the respiration rate (i.e., species other than OM and O_2,

112   Eq. (2). If a reactant concentration falls below a threshold concentration, the respiration rate is inhibited. Reactant

113   inhibition is computed by Eq. 5 (Kinzelbach et al., 1991) for reactant species j:

114      $I_j = 0.5 + \frac{arctan([C_j]-C_{th_j})\cdot f}{\pi}$,   (5)

115   where $C_{th,i}$ is the threshold concentration [M], f is the threshold scaling factor [-]. The default C_{th_j} is 10^{-20} M.

116   The reaction rates are also inhibited by the microbial carrying capacity of the system, I_{cc}, as follows in Eq. (6):

117      $I_{CC} = 1 - \frac{[BM]}{CC}$ (6)

118   where [BM] is the biomass concentration [mol-BM·L^{-1}], CC is the biomass carrying capacity [mol-BM·L^{-1}]. I_{cc} has a

119   non-negativity constraint, so if [BM] > CC, then $I_{cc} = 0$.

120   These inhibition factors are applied to the overall rate expression as shown in Eq. (7).

121 $r_{i,inhibited} = r_i I_{CC} \prod I_j \quad \forall y_{i,j} < 0,$ (7)

122 The overall individual species rates, $d[C_j]/dt$, [mol-species$\cdot$L$^{-1}\cdot$hr^{-1}] are then computed as follows with Eq. (8):

123 $\frac{dC_j}{dt} = (\sum_{i=1}^{n} y_{i,j} r_{i,inhibited})[BM],$ (8)

124 where j is the species index. The total number of species includes 7 general species (i.e., HCO$_3^-$, NH$_4^+$, HPO$_4^-$, HS$^-$,

125 H$^+$, O$_2$, BM (i.e., Eq (1)) and the OM species considered (i.e., typically 10). i is the reaction index, n is total number

126 of reactions as based on the total number of OM species (typically, with this workflow $n = 10$). $y_{i,j}$ is the coefficient

127 for species j in reaction i.

128
129 The expression for biomass is also modified to account for biomass decay (note all biomass stoichiometries are 1 by

130 definition):

131 $\frac{dBM}{dt} = (\sum_{i=1}^{n} y_{i,j} r_{i,inhibited})[BM] - k_{deg}[BM],$ (9)

132 where k_{deg} is the biomass decay rate [hr^{-1}].

133

134 **2.2 Lambda Analysis and Binning**

135 To reduce the number of organic compounds considered in the simulation, OM molecules are grouped, or binned,

136 based on their λ value computed by Eq. (10):

137 $\lambda = \frac{\Delta G_{r,anabolic} + \Delta G_{r,dissipation}}{(-\Delta G_{r,catabolic})},$ (10)

138 where ΔG are the Gibbs energies for the anabolic and catabolic reactions and the associated dissipation energy,

139 respectively. The value of λ is indicative of how many times the catabolic reaction needs to be completed to provide

140 the energy required to synthesis one mole of biomass. Lower λ values suggest higher thermodynamic favorability of

141 OM respiration. Using the chemical formula determined for each OM molecule, the energy balance equations are

142 solved providing the overall reaction stoichiometry Eq. (1) and the λ is calculated. Using the λ value for each molecule,

143 the cumulative probability distribution for the sample is produced (Figure 2).
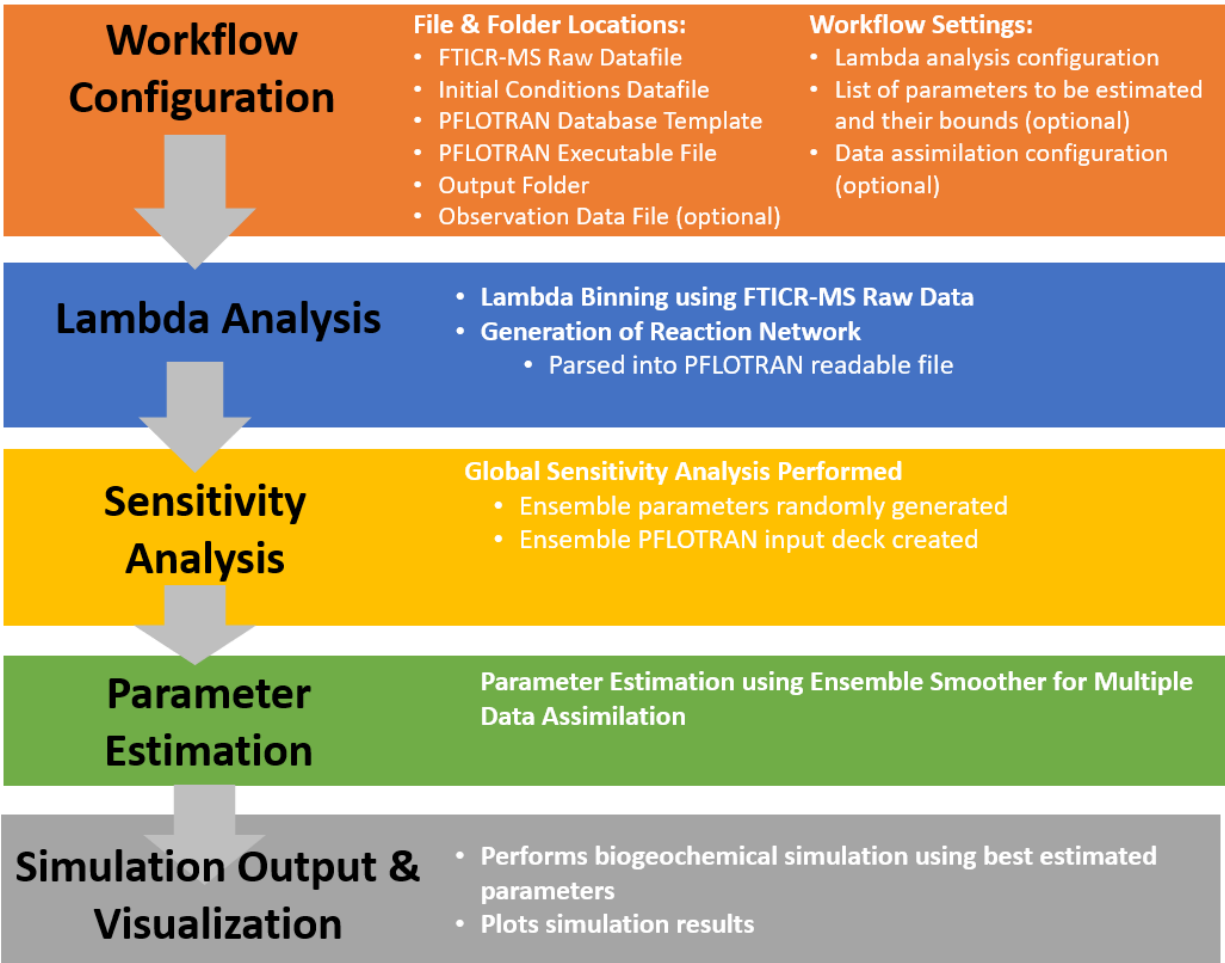
Figure 1: Flow Chart of the Lambda-PFLOTRAN Workflow.

It is this conversion from individual compounds to a distribution that is critical for reducing the entire sample down to a representative set of expressions. The λ bins are then formed by splitting the cumulative probability distribution into equally weighted sections as which to define the overall sample by. The illustrative example shown in Fig. 2 demonstrates the sample distribution being divided into 10 sections (i.e., in this case each section contains 10% of the overall sample distribution).
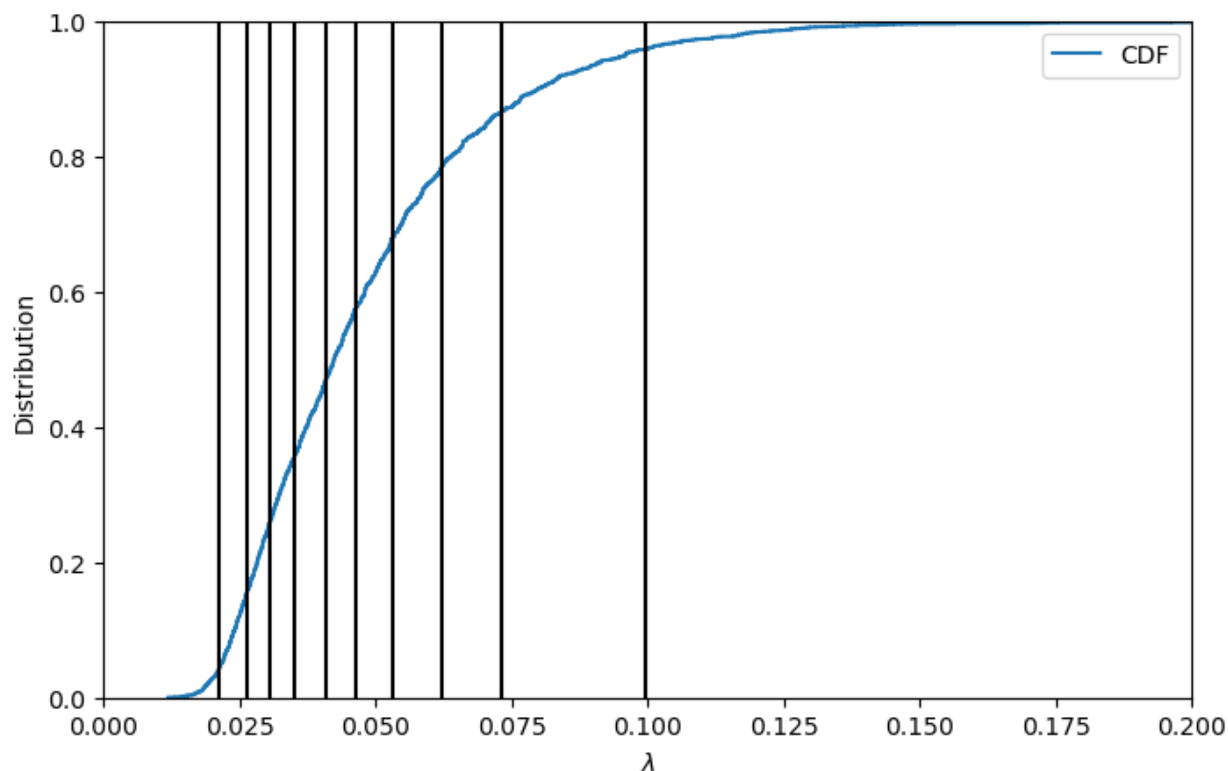
152

153 **Figure 2:** Lambda binning to convert raw FTICR-MS into a representative reaction network using the cumulative probability

154 distribution function (CDF) for Test Case 1a. Vertical lines display the average λ value for each of the 10 bins (left to right, λ bin

155 1 to 10).

156

157 Each section is used to determine a representative organic matter formula and the associated reaction and

158 stoichiometry of that λ bin. The group of representative reactions (one per bin) is called the reaction network. A

159 demonstrative reaction network defined by λ analysis and binning is shown in Table 1.

160

161 **Table 1:** Reaction Network Developed from Lambda Theory for Test Case 1a

Bin Number	Representative Organic Matter Species Formula	λ	y_{OM}	y_{HCO3^-}	y_{NH4^+}	$y_{HPO4^{--}}$	y_{HS^-}	y_{H^+}	y_{O2}
1	$C_{31}H_{44}N_{0.33}O_{4.8}P_{0.6}S_{0.3}$	0.021	-0.05	0.64	-0.17	-0.18	0.03	0.02	-1.07
2	$C_{26}H_{39}N_{0.20}O_{7.0}P_{0.6}S_{0.1}$	0.026	-0.07	0.68	-0.10	-0.19	0.04	0.01	-1.06
3	$C_{22}H_{36}N_{0.24}O_{7.5}P_{0.5}S_{0.1}$	0.031	-0.08	0.69	-0.02	-0.18	0.04	0.01	-1.06
4	$C_{20}H_{32}N_{0.28}O_{7.3}P_{0.4}S_{0.1}$	0.035	-0.08	0.72	-0.08	-0.18	0.04	0.01	-1.05
5	$C_{19}H_{29}N_{0.48}O_{7.9}P_{0.3}S_{0.2}$	0.041	-0.09	0.79	-0.17	-0.16	0.03	0.02	-1.04
6	$C_{18}H_{26}N_{0.68}O_{8.1}P_{0.2}S_{0.2}$	0.046	-0.10	0.85	-0.27	-0.13	0.02	0.02	-1.03
7	$C_{17}H_{24}N_{0.69}O_{8.1}P_{0.2}S_{0.2}$	0.053	-0.11	0.90	-0.32	-0.12	0.02	0.02	-1.02
8	$C_{15}H_{20}N_{0.67}O_{7.6}P_{0.2}S_{0.2}$	0.062	-0.13	0.94	-0.42	-0.11	0.02	0.03	-1.00

| 9 | $C_{13}H_{19}N_{1.13}O_{87.4}P_{0.1}S_{0.2}$ | 0.073 | -0.15 | 1.01 | -0.48 | -0.03 | 0.01 | 0.03 | -1.00 |
| 10 | $C_{10}H_{15}N_{1.56}O_{6.5}P_{0.1}S_{0.2}$ | 0.100 | -0.21 | 1.17 | -0.75 | 0.12 | 0.01 | 0.04 | -0.97 |

162

163   Currently, the representative OM molecule that defines each bin is computed as the average chemical formula of all

164 the molecules present in that λ section. The disadvantage of this approach is that unrealistic compounds are defined

165 as representative molecules instead of realistic molecules. The issue with selecting a single, but real compound, from

166 within each λ section resides in chemical complexity and variation - for instance some molecules may contain low

167 levels of phosphorous or sulfur and others may not contain either element in the chemical formula. Thus, requiring

168 the representative chemical formula to be a real compound present in the sample would create basis which would

169 propagate through the reaction network and into the resulting biogeochemical simulation results.

170 **2.3 Lambda-PFLOTRAN Workflow**

171   The Lambda-PFLOTRAN workflow digests raw FTICR-MS data, calculates the λ distribution for the sample,

172 generates the λ bins and corresponding reaction network, and completes a biogeochemical simulation using

173 PFLOTRAN. Further, we incorporated sensitivity analysis and ensemble data assimilation to enable an in-depth

174 exploration of the impact of reaction parameters on respiration as well as a straightforward parameter estimation

175 method to fit model parameters to experimental data.

176   The workflow is implemented through a user-friendly Jupyter notebook interface (Kluyver et al., 2016) where a user

177 can configure the simulation parameters by adjusting initial concentrations, λ binning configuration, parameter values

178 and/or ranges, and data assimilation options. Based on the user's data file and the associated parameters, scripts within

179 the Jupyter notebook write the corresponding PFLOTRAN input files, including OM molecules and aqueous

180 chemistry. The PFLOTRAN simulations are completed locally through a Docker container making this capability

181 much more user-friendly and accessible. The progress of the data assimilation tool used for parameter fitting is

182 illustrated within the Jupyter notebook. The resulting best fit final biogeochemical simulation is output visually with

183 plots and as a text file (when applicable).

184   The Lambda-PFLOTRAN workflow steps are shown in Figure 1 and described in detail in the following subsections:

185 **2.3.1 Step 1 – Workflow configuration**

186   The first step is to set up the workflow configuration for a Lambda-PFLTORAN application. This includes specifying

187 the file and folder locations of the following information: 1) FTICR-MS raw data file (.csv), 2) initial species

188 concentrations file (.csv) that includes starting molar concentrations for HCO_3^-, NH_4^+, HPO_4^{2-}, HS^-, H^+, O_2 (aq), BM

189 and total organic carbon (TOC), 3) PFLOTRAN database template file, 4) PFLOTRAN executable file, 5) workflow

190 output folder, and if completing parameter estimation, (6) the data observation file (.csv), if applicable.

191   The user is also asked to configure workflow settings related to: (1) the lambda analysis configuration, including

192 number of λ bins and method to define the λ bins (i.e., cumulative vs uniform); (2) the respiration modeling parameter

setup, including the list of the parameters to be estimated and their associated upper and lower bounds and (3) the data assimilation configuration (see below).

2.3.2 Step 2 – Organic Matter Chemistry using Lambda Analysis

With only an input of FTICR-MS data, the workflow first performs the lambda analysis (Section 2.2) to group OM molecules into various λ bins based on each compound's thermodynamics (Figure 2) and produce the corresponding reaction network for respiration (Table 1). The default number of λ bins is 10, although this can be adjusted in the workflow configuration by the user, if desired. The generated reaction network is then automatically parsed by the workflow into a text file that can be read by PFLOTRAN.

2.3.3 Step 3 – Sensitivity Analysis using Mutual Information

This step performs the global sensitivity analysis on the parameters to be estimated. Ensemble parameters are first generated by randomly sampling from their predefined ranges in the configuration step and saved into an HDF5 file. Then, the workflow generates a PFLOTRAN input deck to conduct ensemble simulations using the ensemble parameters. The generated ensemble model states enables a global sensitivity analysis using mutual information (Cover and Thomas, 2006; Jiang et al, 2022) as follows:

$$I(X;Y) = H(Y) - H(Y|X) = \sum_{X=x}\sum_{Y=y} p(x,y) log\left(\frac{p(x,y)}{p(x)p(y)}\right), \tag{11}$$

where x and y are the specific values of X and Y, respectively; $H(Y)$ is the Shannon's entropy of Y; $H(Y|X)$ is the conditional entropy of Y given X; p is the probability density function. Higher I indicate stronger sensitivity between X and Y. Besides sensitivity analysis, the ensemble parameter/states also serve as the prior information for parameter estimation at the next step.

2.3.4 Step 4 – Parameter Estimation using Ensemble Smoother for Multiple Data Assimilation

The workflow adopts Ensemble Smoother for Multiple Data Assimilation (Emerick and Reynolds, 2013; Jiang et al, 2021), abbreviated as ESMDA, for data assimilation in this step. Rooted in ensemble Kalman filter, ESMDA is an iterative data assimilation approach that assimilates the observations on the entire time period for multiple times to reduce the uncertainty of the estimated or posterior parameters. During each iteration of ESMDA, the model parameters are updated based on the following equation:

$$m_{k,l}^u = m_{k,l}^f + C_{MD,l}^f \left(C_{DD,l}^f + \alpha_l C_D\right)^{-1}\left(d_{obs} + \sqrt{\alpha_l}C_D^{\frac{1}{2}}z_k - d_{k,l}^f\right),\ k = 1,\dots,N_e\ and\ l = 1,\dots,L, \tag{12}$$

where the subscripts k and l are the indices of the ensemble member and the iteration, respectively; the superscripts u and f are the updated and forecast parameters or states, respectively; N_e is the number of ensemble members; L is the number of iterations; $m_{k,l}^f$ and $m_{k,l}^u$ are the kth ensemble member of the forecast/prior and updated/posterior parameters, respectively, at the lth iteration; d_{obs} is the observation; z_k is the observation noise sampled from

223   independent standard normal distributions for the kth ensemble member; $d^f_{k,l}$ is the kth ensemble member of the

224   predicted observation states by the model using $m^f_{k,l}$; $C^f_{MD,l}$ is the cross-covariance matrix between the prior parameters

225   m^f_l and the predicted observation states d^f_l; $C^f_{DD,l}$ is the auto-covariance matrix of the predicted observation states d^f_l;

226   C_D is the auto-covariance matrix of the observation error; and α_l is the inflation coefficient at the lth iteration with the

227   sum of all α_l equal to one.

228

229   Here, the assimilation starts with taking the ensemble model parameters/states in Step 3 and the provided observations,

230   and calculates the posterior parameters using ensemble Kalman filter, updates the prior parameters with the current

231   posterior for the next iteration, and then repeats the whole process for multiple times (typically 3 to 5 iterations, as

232   defined by the user). The final estimated parameters are obtained from the posterior parameter at the last iteration and

233   are updated in the parameter HDF5 file. The parameter estimation is implemented in a way that allows assimilating

234   either a single (e.g., Test Case 1) or multiple observed species simultaneously through a simple change of the inputs.

235   For example, if temporal experimental or field data is available for oxygen, pH, and total carbon, all these data sources

236   could be simultaneously fit to, with only minor adjustments to Jupyter notebook.

2.3.5 Step 5 – Simulation Output and Visualization

238   The last step performs the ensemble simulation of the biogeochemical modeling a final time using the estimated

239   parameters in Step 4. Optionally, users can further pick the realization with the best performance. The user has the

240   option to select their preferred goodness of fit metric from the following options as a means for selecting the best

241   performing simulation: R-squared (R^2), Root Mean Squared Error (RMSE), Modified Kling-Gupta Efficiency

242   (mKGE), Nash-Sutcliffe Model Efficiently Coefficient (NSE), or Correlation Coefficient (CorC). Based on the

243   selection, the final time series of aqueous chemistry, oxygen consumption, CO_2 production, and lambda binned, and

244   total organic carbon concentrations will be computed and plotted.

3 Test Cases

3.1 Test Case 1 - Oxygen Depletion Incubation Experiments.

247   In the first illustrative example, the workflow was used to fit μ_{max} to laboratory incubation experiments where oxygen

248   levels were measured over two hours in a closed reactor. The incubation experiments were completed as part of the

249   Worldwide Hydrobiogeochemistry Observation Network for Dynamic River Systems (WHONDRS) program

250   (Goldman et al, 2020). For these incubations, sediment was taken from three locations within a stream (i.e., upstream

251   [Test Case 1a], midstream [Test Case 1b], and downstream [Test Case 1c]) in the Yakima River Basin in Washington,

252   USA for subsequent laboratory respiration experiments. FTICR-MS was used to determine the OM chemistry from

253   each sediment sample, resulting in variable formulae being identified in each sample. Formula assignments for all the

254   samples included herein were completed using formultitude (Tolic et al., 2017). Total dissolved organic carbon

255   concentration paired with the FTICR-MS sample and biomass measurements taken at the start of each experiment

256   were used as the initial concentrations for each of the simulations. Due to the absence of quantitative data related to

257 how the total carbon mass is distributed between various the OM compounds, the total carbon concentration (on a per-

258 C basis) was assumed to be split equally between each of the λ bins. The total organic carbon concentration was

259 distributed into each λ bin using Eq. (13). While this assumption results in equal distribution of carbon between the

260 bins, consequently, it assigns different initial species concentrations due to varying carbon concentrations between the

261 molecules.

262 $$[C_{\lambda\text{bin}}]_0 = \frac{[TOC]}{n_{\lambda bin} nC_{\lambda bin}} \tag{13}$$

263 Where: $[C_{\lambda\text{bin}}]_0$ is the initial species concentration in each λ bin [mol·L^{-1}]; TOC is the total organic carbon measured

264 [mol-carbon·L^{-1}]; $n_{\lambda bin}$ is the number of λ bins [-]; and $nC_{\lambda bin}$ is the number of carbon molecules in the assumed

265 formula for the λ bins [mol-carbon · mol-molecule^{-1}].

266 Using the Lambda-PFLOTRAN workflow, the FTICR-MS data from each laboratory experiment was digested into

267 the corresponding λ bins to create the individual reaction network. The Jupyter Notebook for this example is

268 "Test_Case1-WHONDRS.ipynb" and is available at https://doi.org/10.15485/2281403.

269

270 μ_{max} was fit to the provided experimental oxygen data. The final lambda binned fit, along with corresponding carbon

271 consumption (individual and total) and aqueous chemistry is displayed in Figure 3 (and in the supporting information

272 Fig. S1 and S2 for Test Cases 1b [midstream] and 1c [downstream], respectively). To evaluate the use of lambda

273 binned OM obtained from FTICR-MS (Figure 3), the workflow was also run for a baseline case where μ_{max} was fit

274 again, but this time assuming a generic bulk OM form of CH_2O for comparison. The reaction network developed for

275 a generic OM molecule of CH_2O is shown in Eq. 14.

276 $$2.03\ CH_2O + 0.98\ O_2 + 0.2\ NH_4^+ \rightarrow 1.03\ HCO_3^- + 1.23\ H^+ + 0.4\ H_2O + CH_{1.8}O_{0.5}N_{0.2} \tag{14}$$
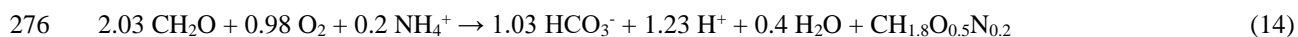
277 This reaction network is used in the Lambda-PFLOTRAN workflow for bulk OM simulations.

278 Fitted μ_{max} values for the lambda binned model is 0.25 min^{-1} ($R^2 = 0.99$) and fitted μ_{max} to the bulk OM CH_2O model

279 is 0.032 min^{-1} ($R^2 = 0.96$). V_h and CC are fixed at assumed values of 10 m^3 and 1 M, respectively in both simulations.

280
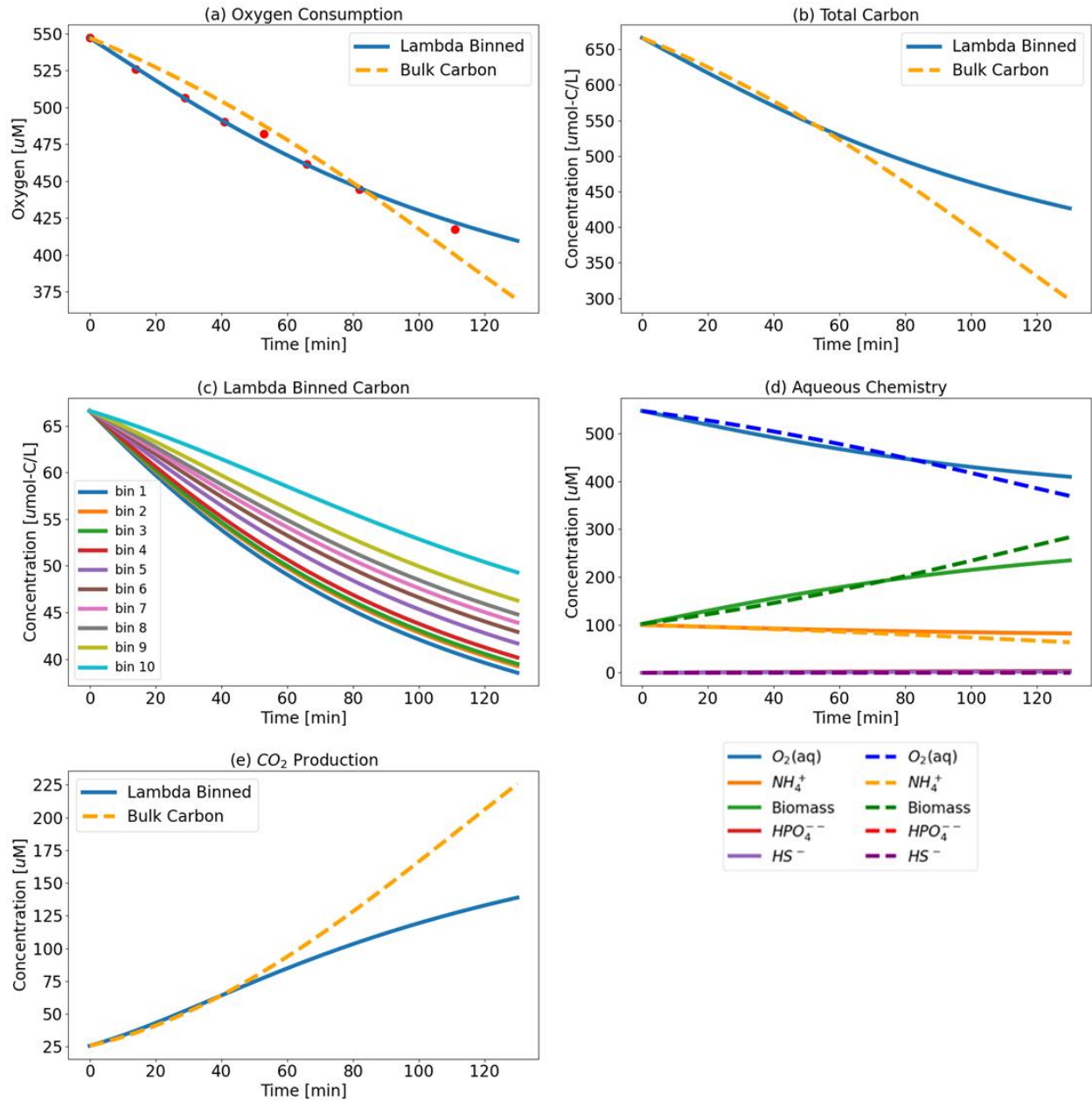
Figure 3: Test Case 1a Results – (a) Oxygen Consumption where Lambda-PFLOTRAN workflow was used to fit (blue line) to experimental respiration data (red dots) and (b) Total Carbon Consumption; (c) Individual Organic Matter Consumption by λ bin; and (d) biogeochemistry including O_2 (aq) (blue); Biomass (green); NH_4^+ (orange); HS^- (purple); and HPO_4^- (red); and (e) CO_2 production for the upstream incubation. The dashed orange lines (in a, b and e) show simulation results assuming a generic OM species of CH_2O for comparison.

However, even over the short time frame of this simulation (i.e., only 120 minutes), the difference between assuming the generic CH_2O and using the more detailed organic matter chemistry resulted in different predictions of total carbon and CO_2 generation. The bulk OM model predicts more carbon consumption and greater CO_2 production than the lambda binned model. The bulk OM model estimates that 50% of the initial total carbon is consumed over the first

290   120 mins, whereas the lambda binned model predicts 34% consumption. Similarly, the bulk OM model estimates

291   approximately 35% more CO_2 generation as compared the lambda binned model. The effects on aqueous chemistry

292   over this short duration are more muted, albeit still present.

293   **3.2 Test Case 2 - Respiration Incubation Experiments.**

294   Test Case 2 uses soil respiration incubation data from Ward et al. (2023) aimed at investigating the influence of soil

295   type, oxygen condition (aerobic vs. anaerobic), and seawater exposure (fresh vs. saline) on respiration extent and rate.

296   For these experiments, temporal measurements were collected for CO_2 generation, dissolved organic carbon (DOC),

297   organic matter formulas via FTICR-MS and other bulk aqueous chemistry (i.e., pH, NH_4^+, and other metals and ions)

298   creating a rich dataset for calibration of system specific lambda model parameters. These incubations were setup by

299   adding dry soil to the reactor and then adding water (resulting in a soil:water ratio ranging from 1:11 to 1:16). The soil

300   and water were shaken vigorously for five minutes, and then sampled for the initial time point prior to officially

301   starting the incubation. For the aerobic experiments, the reactor headspace was cycled every 24 hours to measure CO_2

302   generated but also to ensure the system was kept aerobic; this was only performed five days per week, with no

303   measurements taken on the weekend due to logistical constraints. Upon experiment completion, the increase in DOC

304   concentrations indicated organic carbon was being kinetically released from the soil into the aqueous phase over the

305   course of the 21-day experiment. Similarly, measured NH_4^+ concentrations also increased during the experiment. To

306   address this within our reactive transport model, a source of nitrogen was assumed to be released from the soil as well

307   ($N_{release}$). Both carbon and nitrogen release are included in this example and are assumed to follow a zero-order constant

308   release rate. Any organic carbon released from the soil was fractionated into each λ bin on the same per-carbon basis

309   assumed for the initial total organic carbon. This was implemented through a dependent function that calculated the

310   release of carbon into each λ bin based on a fitted single bulk $k_{release}$ rate. Mathematically in PFLOTRAN the constant

311   oxygen conditions were implemented through a gas-liquid partitioning expression with a fast exchange term. These

312   three additional processes were added to describe the experimental conditions of Test Case 2 more accurately (i.e.,

313   release of carbon, nitrogen and sustained aerobic conditions); however, a PFLOTRAN input deck can be expanded

314   and customized to include a host of additional processes and full geochemistry for a specific system of interest. For

315   instance, aqueous complexation, mineral dissolution and precipitation, sorption, and redox reactions can be added, all

316   of which can influence the resultant pH and carbon, nitrogen, and other nutrient dynamics.

317   The workflow was used to fit μ_{max}, V_h, CC, k_{deg}, as well as $k_{release}$, to the temporal CO_2 generation for a single aerobic

318   soil incubation (Figure 5). The Jupyter Notebook for this example is "Test_Case2-Colloids.ipynb".

319
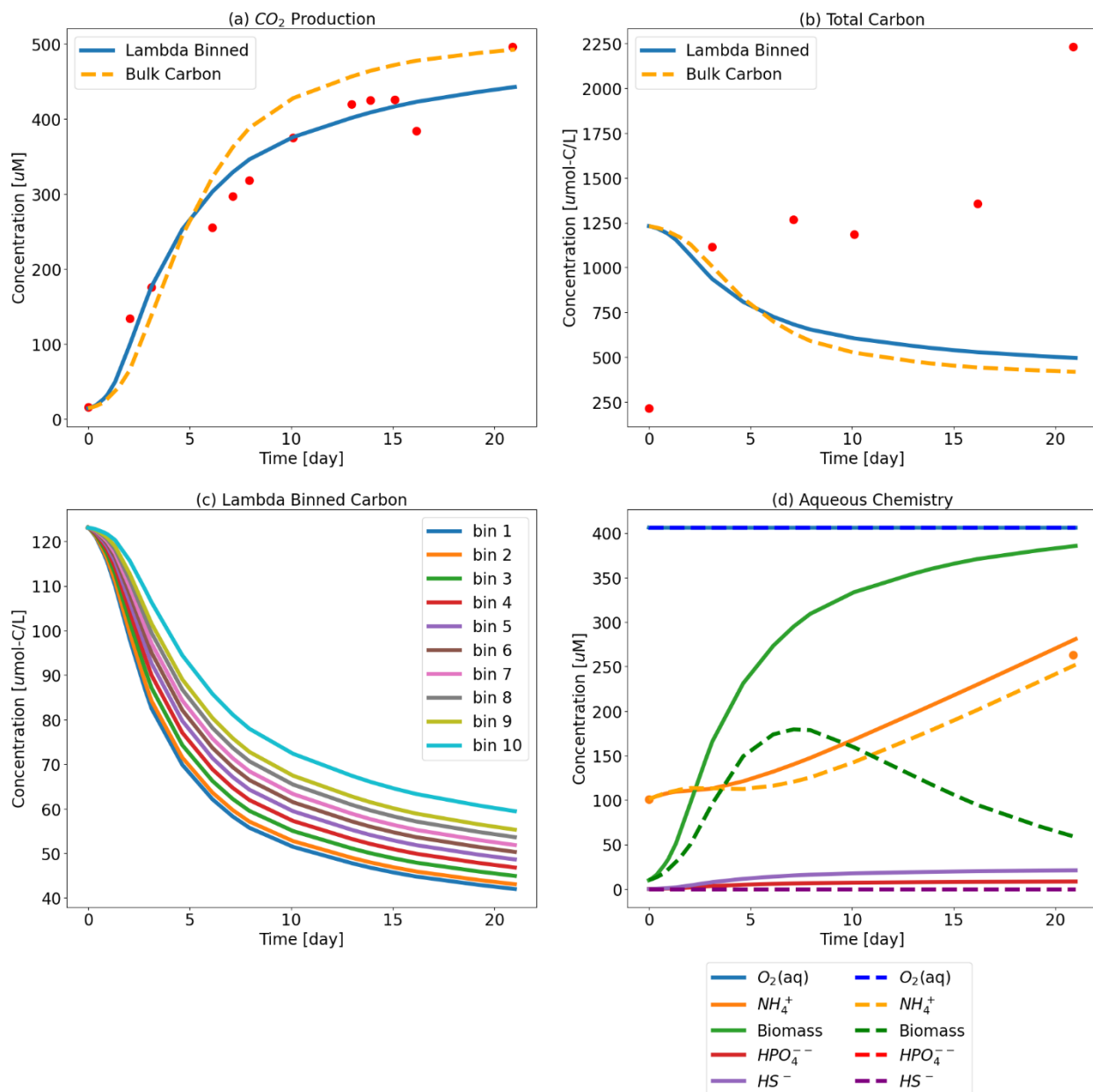
321 **Figure 4.** Test Case 2 Results – (a) CO_2 production where Lambda-PFLOTRAN workflow was used to fit (blue line) to
322 experimental respiration data (red dots) and (b) the corresponding Total Organic Carbon; (c) Individual Organic Matter
323 Consumption by λ bin, and (d) the corresponding biogeochemistry including O_2 (aq) (blue); Biomass (green); NH_4^+ (orange); HS^-
324 (purple); and HPO_4^{--} (red). Dots indicate experimental data. The dashed orange lines in the top two figures show simulation results
325 assuming a generic OM species of CH_2O for comparison. Fitted parameters for lambda binned model are $k_{release} = 5.5 \times 10^{-12}$ day^{-1};
326 $\mu_{max} = 37.6$ day^{-1}, $V_h = 5.0$ m^3, CC = 0.12 M, and $k_{deg} = 1 \times 10^{-3}$ day^{-1} ($R^2 = 0.953$) and fitted bulk OM CH_2O model values are $k_{release}$
327 $= 2.0 \times 10^{-12}$ day^{-1}; $\mu_{max} = 47$ day^{-1}, $V_h = 1.0$ m^3, CC = 0.77 M, and $k_{deg} = 0.15$ day^{-1} ($R^2 = 0.909$).

328

329 For the purposes for showcasing the workflow, five parameters were estimated in this test case example, and as a
330 result the models are over parametrized given the amount of data available. Parameter sensitivity over the course of

331   simulation time is shown in Figure 5 and suggests this system is highly sensitive to V_h. It should be noted that both

332   these model fits are also highly sensitive to the allowable parameter space as user defined by the lower and upper

333   parameter bounds. In general, parameterization efforts are inherently challenging. For Lambda-PFLOTRAN, which

334   models microbially mediated processes, it is recommended to initially focus on constraining biomass parameters (i.e.,

335   CC, k_{deg}, and V_h) by measuring temporal changes in biomass concentrations. Further, V_h and μ_{max} are typically highly

336   sensitive and often correlated. However, since V_h represents the theoretical volume accessible to microbes and cannot

337   be directly measured, it is suggested to fix V_h within a range of 1-10 m³. If these microbial parameters can be

338   adequately constrained, focus can shift to μ_{max}, the maximum microbial growth rate, which significantly influences

339   overall respiration and is expected to exhibit the highest variability across different locations and conditions.
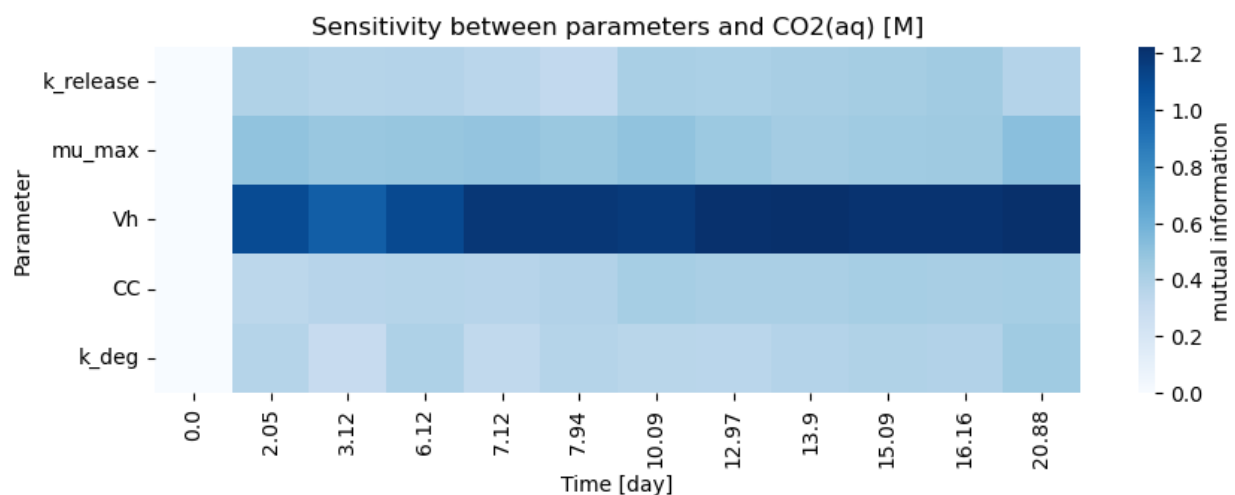
340

341   **Figure 5.** Test Case 2 - Sensitivity Analysis Output during Parameter Estimation. The sensitivity of five fitted parameters ($k_{release}$,

342   μ_{max}, V_h, CC, and k_{deg}) on temporal aqueous CO_2 concentrations as a function of time.

343   Any additional experimental data, either collected during incubations or through independent experiments (e.g.,

344   carbon release from the soil in an abiotic system), would be expected to help constraint the model and improve

345   parameterization. Additionally, it is unclear why the model is unable to capture the total organic carbon behavior in

346   Test Case 2. One potential explanation is that some of the released organic carbon may not be fully bioavailable and

347   thus the model may be compensating for this by artificially reducing the concentration of OM available for respiration.

348   **4 Variability and Impact of Organic Matter Speciation**

349   The variability in OM speciation was briefly assessed by comparing FTICR-MS data from Test Cases 1 and 2. Each

350   identified OM species was classified into one of nine compound classes. For Test Case 1, the average of the three Test

351   Case 1 samples (1a - upstream, 1b - midstream, and 1c - downstream) was computed. The predominant classes were

352   proteins ($34 \pm 1\%$), lignin ($26 \pm 1\%$), and lipids ($13 \pm 2\%$), with the errors representing the standard deviation among

353   the Test Case 1a-c samples. The low standard deviation suggests consistent reproducibility in OM speciation for

354 samples taken from nearby locations. In contrast, OM in Test Case 2 was primarily composed of lignin (37.4%) and

355 concentrated hydrocarbons (32%). The full distribution of compound classes is presented in Figure 5.
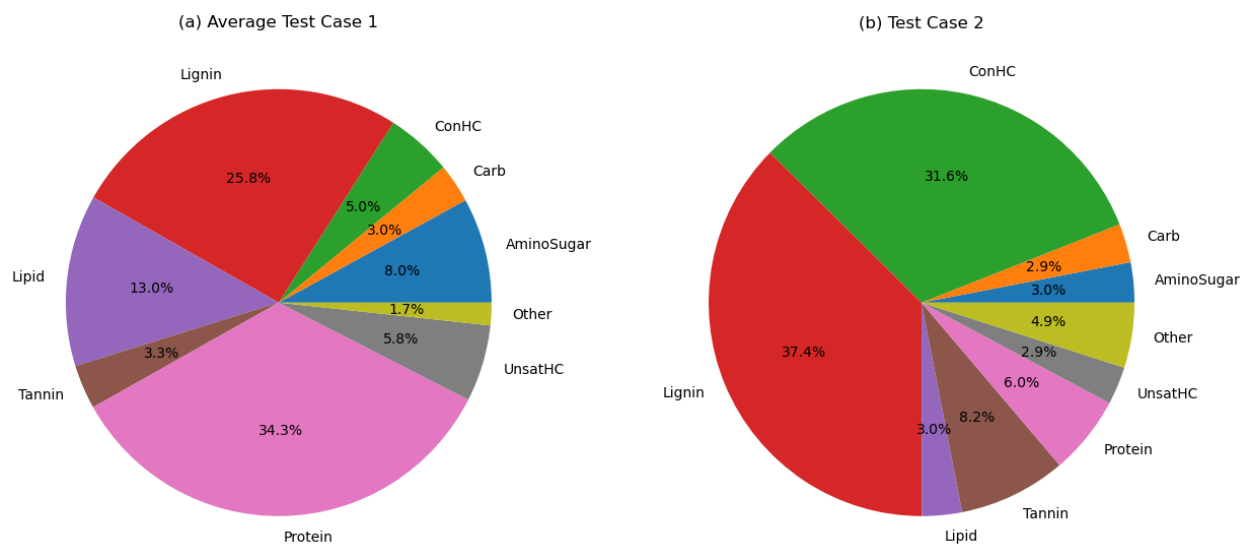
356

357 **Figure 5.** Distribution of Organic Matter Compound Classes: (a) Test Case 1 and (b) Test Case 2.

358 Note: Test Case 1 is the average of Test Case samples 1a-c. ConHC = Condensed Hydrocarbon; UnsatHC = Unsaturated

359 Hydrocarbon

360

361 The influence of the sample OM speciation on the λ binned reaction networks was also assessed. Figure 6 illustrates

362 the impact of OM speciation on the corresponding λ binned reaction networks, with three key observations. First, the

363 variability in OM speciation between different samples is evident when comparing Test Case 1 and Test Case 2. To

364 enhance visual clarity, the range of Test Case 1 samples (1a-c) is depicted as a grey shaded region, showing the spread

365 between the minimum and maximum values of the three samples. For Test Case 2, data from the single FTICR-MS

366 sample is represented by blue dots. Test Case 1 and 2 have distinct λ derived reaction networks as indicated by the

367 little overlap between the grey region and the blue dots in Figures 6b-i.

368
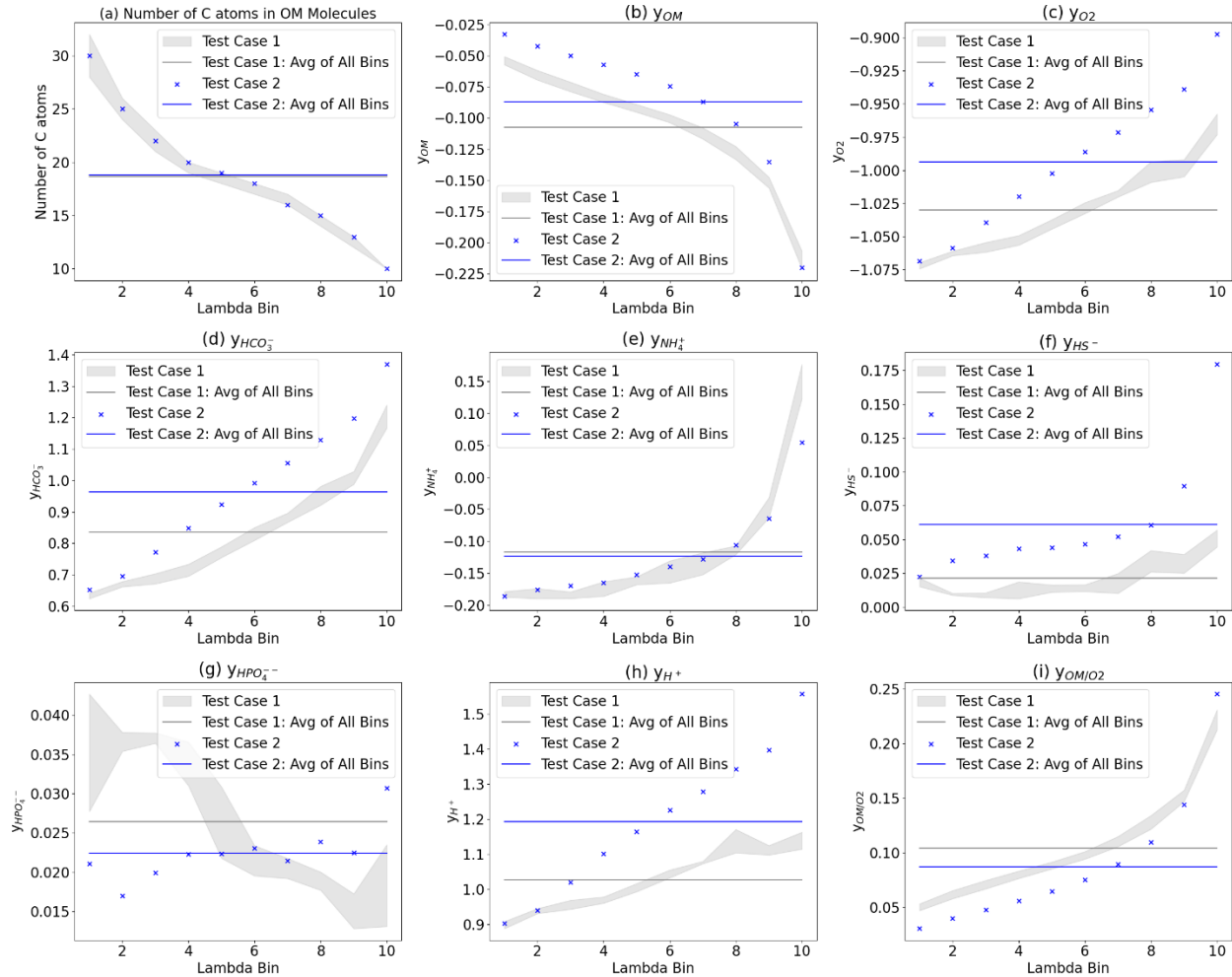
Figure 6. Comparison of Lambda-Binned Reaction Network Parameters: (a) number of carbons in the OM; stoichiometric coefficient, y, for (b) OM, (c) O_2, (d) HCO_3^-, (e) NH_4^+, (f) HS^-, (g) HPO_4^{--}, (h) H^+; and (i) ratio of OM/O_2 coefficients for Test Case 1a-c (grey dots); the average of all λ bins for Test Case 1 (grey line); Test Case 2 (blue x); and the average of all λ bins for Test Case 2 (blue line). The grey shaded area highlights the range of values for Test Case 1a-c for better visual comparison.

Second, the λ binning process captures the OM speciation variation within a sample. To illustrate this intrasample variability, a line representing the average of all λ bins is shown on Figure 6 (grey line for Test Case 1, blue line for Test Case 2). The difference between the reaction network coefficients (vertical axis) for the λ binning (grey shaded area and blue dots) and the Test Case average lines highlights the extent of this variability. Finally, although the λ binning process resulted in a similar number of carbon atoms to OM molecules within each λ bin for both test cases (Figure 6a), the resulting stoichiometric coefficients in the reaction networks differ significantly (Figures 6b-h). These stoichiometric differences lead to variations in biogeochemical outcomes, such as OM-to-oxygen utilization ratios during aerobic respiration (Figure 6i). These differences are due to the additional elements beyond carbon in the OM molecules (i.e., nitrogen, oxygen, sulfur, hydrogen, and phosphorus).

385 To further assess and isolate the effect of OM speciation, extended forward simulations were performed by only

386 varying FTICR-MS input data (Figure 7). FTICR-MS samples from Test Cases 1a-c and Test Case 2 were tested.

387 These simulations replicate Figure 3 (i.e., Test Case 1a conditions and fitted μ_{max} values) with the expectation of OM

388 speciation, and demonstrate the significant impact of OM chemistry and speciation on overall predicted behavior,

389 especially over longer time periods.

390
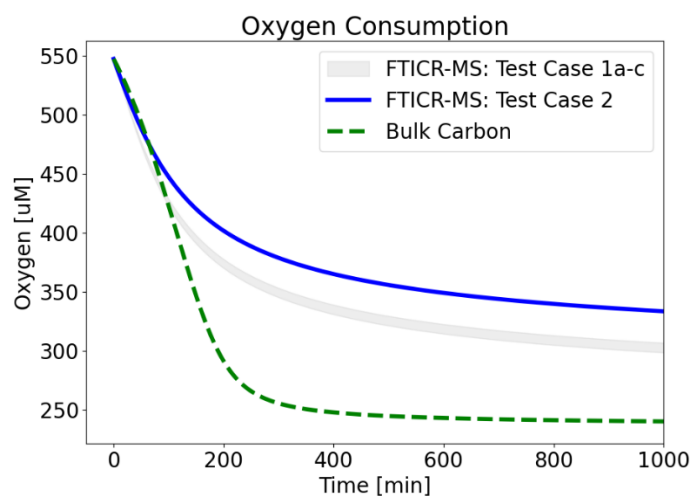
391

392 **Figure 7.** Influence of OM Speciation on Oxygen Consumption. FTICR-MS data from Test Cases 1a-c (grey shaded area), and

393 Test Case 2 (blue line) were used as inputs. Bulk CH_2O OM (green line) was also plotted for reference. Best fit μ_{max} values to Test

394 Case 1a were used (i.e., lambda binned $\mu_{max} = 0.25$ min^{-1}; bulk OM $\mu_{max} = 0.032$ min^{-1}).

395

396 The clear variability in OM speciation, differences between a generic OM reaction network and one informed by

397 FTICR-MS, and the impact of OM chemistry on biogeochemical predictive simulations underscore the importance of

398 incorporating site-specific OM chemistry informed by ultra high resolution characterization into biogeochemical

399 models.

400 **5 Conclusions**

401 Overall, Lambda-PFLOTRAN workflow provides an important linkage between molecular scale organic matter

402 characterization and reactive transport simulations. This workflow allows for the influence of organic matter

403 composition to be utilized within simulators to provide a more comprehensive understanding of the system chemistry

404 and behavior, moving beyond the standard assumption of bulk organic matter chemistry and composition. While there

405 are current limitations due to how composition is characterized and quantified, this workflow connecting

406 characterization information to simulations is an important advancement that can be refined as these laboratory

407 techniques improve over time.

408 One of the major limitations surrounding this method, is the lack of understanding of organic matter compound

409 bioavailability, resulting in a large conceptual gap as to how various organic carbon compounds may be utilized by

microbes. In the absence of such information, all identified organic matter molecules are assumed to have equal bioavailability within this modeling framework when, in reality, compounds will exhibit varying degrees of bioavailability depending on factors such as associated size fraction, carbon pool, and environmental factors (Schmidt et al., 2011; Ahamed et al., 2023). Until improved understanding is established to discern individual compound bioavailability, this will remain as a limitation.

Another limitation of this method resides around the analytical limitations of organic carbon characterization and quantification. For instance, FTICR-MS focuses on water soluble organic matter which may provide a basis in the types of carbon identified by this technique (Tfaily et al., 2017). Additionally, as mentioned previously, FTICR-MS is qualitative, it does not provide structural information and will not differentiate between different isomers that have the same molecular formulas, it is only able to identify molecular formula is present or absent and not the concentration associated with each peak. Here, this has been addressed by assuming equal distribution of total carbon between the formulas within each λ bin on a per-carbon basis. This caveat can be easily updated in the workflow if new analytical advances are made that provide more quantitative information. Some existing approaches could be suitable for this type of modeling such as using quantitative biomarkers that cover major compound classes (Kim and Blair, 2023); but further advances in obtaining both high resolution and quantitative OM characterization would greatly aid in how we understand and model ecosystems.

Acknowledgements:

This research was performed under a variety of interdisciplinary projects including the U.S. Department of Energy (DOE) sponsored Office of Science, Office of Biological and Environmental Research (BER), Environmental System Science (ESS) Program, IDEAS-Watersheds, River Corridor Scientific Focus Area (SFA), the Environmental Molecular Sciences Laboratory User Facility sponsored by the Biological and Environmental Research program under Contract No. DE-AC05-76RL01830, and COMPASS-FME, a multi-institutional project supported by DOE-BER as part of the Environmental System Science Program. This study used data from the Worldwide Hydrobiogeochemistry Observation Network for Dynamic River Systems (WHONDRS). This paper describes objective technical results and analysis. The work was performed at the Pacific Northwest National Laboratory (PNNL). PNNL is operated for DOE by Battelle Memorial Institute under contract DE-AC05-76RL01830. This paper describes objective technical results and analysis. Any subjective views or opinions that might be expressed in the paper do not necessarily represent the views of the U.S. Department of Energy or the United States Government.

Code Availability:

The source code, installation requirements, example test case notebooks, and associated data are available in ESS DIVE at https://doi.org/10.15485/2281403

Author Contribution:

KM: conceptualization, formal analysis, methodology, software, writing- original draft preparation; PJ: methodology, software, writing- original draft preparation; GH: methodology, software, writing-review & editing; TA: data curation, software, writing-review & editing; HS: methodology, writing-review & editing; RK: supervision; NW: supervision, writing-review & editing; MB: investigation; RC: investigation; QZ: investigation; VG: investigation, data curation; AR: investigation; XC: conceptualization, investigation, writing-review & editing

Competing Interests: The authors declare that they have no conflict of interest.

References

Bahureksa, W., Tfaily, M. M., Boiteau, R. M., Young, R. B., Logan, M. N., McKenna, A. M., & Borch, T. (2021). Soil organic matter characterization by Fourier transform ion cyclotron resonance mass spectrometry (FTICR MS): A critical review of sample preparation, analysis, and data interpretation. *Environmental science & technology*, 55(14), 9637-9656, https://doi.org/10.1021/acs.est.1c01135

Cover, T. M., and Thomas, J. A. (2006). Elements of information theory (Wiley series in telecommunications and signal processing). Wiley-Interscience.

Emerick, A.A., Reynolds, A.C. (2013). Ensemble smoother with multiple data assimilation. *Comput. Geosci*. 55, 3–15. https://doi.org/10.1016/j.cageo.2012.03.011.

461 Fatichi, S., Manzoni, S., Or, D., & Paschalis, A. (2019). A mechanistic model of microbially mediated soil

462 biogeochemical processes: a reality check. *Global Biogeochemical Cycles*, *33*(6), 620-648.

463 https://doi.org/10.1029/2018GB006077

464 Garayburu-Caruso, V., Stegen, J., Song, H.-S., Renteria, L., Wells, J., Garcia, W., et al. (2020). Carbon limitation

465 leads to thermodynamic regulation of aerobic metabolism. *Environ. Sci. Technol. Lett*. 7, 517–524.

466 https://doi.org/10.1021/acs.estlett.0c00258

467 Goldman A E ; Arnon S ; Bar-Zeev E ; Chu R K ; Danczak R E ; Daly R A ; Delgado D ; Fansler S ; Forbes B ;

468 Garayburu-Caruso V A ; Graham E B ; Laan M ; McCall M L ; McKever S ; Patel K F ; Ren H ; Renteria L ; Resch

469 C T ; Rod K A ; Tfaily M ; Tolic N ; Torgeson J M ; Toyoda J G ; Wells J ; Wrighton K C ; Stegen J C ; WHONDRS

470 Consortium T (2020): WHONDRS Summer 2019 Sampling Campaign: Global River Corridor Sediment FTICR-MS,

471 Dissolved Organic Carbon, Aerobic Respiration, Elemental Composition, Grain Size, Total Nitrogen and Organic

472 Carbon Content, Bacterial Abundance, and Stable Isotopes (v8). River Corridor and Watershed Biogeochemistry SFA,

473 ESS-DIVE repository. Dataset. doi:10.15485/1729719 accessed via https://data.ess-

474 dive.lbl.gov/datasets/doi:10.15485/1729719 on 2023-12-28

475 Hammond, G. E., Lichtner, P. C., & Mills, R. T. (2014). Evaluating the performance of parallel subsurface simulators:

476 An illustrative example with PFLOTRAN. *Water resources research*, *50*(1), 208-228.

477 https://doi.org/10.1002/2012WR013483

478 Hammond, G.E. (2022) The PFLOTRAN Reaction Sandbox, *Geoscientific Model Development*, 15, 1659-1676,

479 https://doi.org/10.5194/gmd-15-1659-2022.

480 Jiang P., Chen, X., Chen, K., Anderson, J., Collins, N., Gharamti, M. (2021) DART-PFLOTRAN: An ensemble-based

481 data assimilation system for estimating subsurface flow and transport model parameters. *Environmental Modelling &*

482 *Software*, Volume 142, https://doi.org/10.1016/j.envsoft.2021.105074.

483 Jiang, P., Son, K., Mudunuru, M.K. and Chen, X. (2022). Using mutual information for global sensitivity analysis on

484 watershed modeling. *Water Resources Research*, 58(10), https://doi.org/10.1029/2022WR032932

485 Kim, J., Blair, N.E. Biomarker heatmaps: visualization of complex biomarker data to detect storm-induced source

486 changes in fluvial particulate organic carbon. Earth Sci Inform 16, 2915–2924 (2023). https://doi.org/10.1007/s12145-

487 023-01039-y

488 Kinzelbach, W., Schafer, W., and Herzer, J. (1991). Numerical modeling of natural and enhanced

489 denitrification processes in aquifers. *Water Resources Research*, 27(6):1123–1135.

490 https://doi.org/10.1029/91WR00474

491 Kleerebezem, R., & Van Loosdrecht, M. C. (2010). A generalized method for thermodynamic state analysis of

492 environmental systems. Critical Reviews in Environmental Science and Technology, 40(1), 1-54.

493 https://doi.org/10.1080/10643380802000974

494 Kluyver, T., Ragan-Kelley, B., Pérez, F., Granger, B. E., Bussonnier, M., Frederic, J., ... & Willing, C. (2016). Jupyter

495 Notebooks-a publishing format for reproducible computational workflows. *Elpub*, 87-90. 10.3233/978-1-61499-649-

496 1-87

497 Lehmann, J., Hansel, C.M., Kaiser, C. *et al.* (2020). Persistence of soil organic carbon caused by functional

498 complexity. *Nat. Geosci.* **13**, 529–534 https://doi.org/10.1038/s41561-020-0612-3198718

499 Robertson, A. D., Paustian, K., Ogle, S., Wallenstein, M. D., Lugato, E., & Cotrufo, M. F. (2019). Unifying soil

500 organic matter formation and persistence frameworks: the MEMS model. *Biogeosciences*, *16*(6), 1225-1248.

501 https://doi.org/10.5194/bg-16-1225-2019

502 Schmidt, M., Torn, M., Abiven, S. et al .(2011) Persistence of soil organic matter as an ecosystem

503 property. *Nature* 478, 49–56. https://doi.org/10.1038/nature10386

504 Stegen, J. C., Garayburu-Caruso, V. A., Danczak, R. E., Goldman, A. E., Renteria, L., Torgeson, J. M., and Wells, J.

505 R.: Hyporheic Zone Respiration is Jointly Constrained by Organic Carbon Concentration and Molecular Richness,

506 EGUsphere [preprint], https://doi.org/10.5194/egusphere-2022-613, 2023.

507 Song, H.S., Stegen, J.C., Graham, E.B., Lee, J.Y., Garayburu-Caruso, V.A., Nelson, W.C., Chen, X., Moulton, J.D.

508 and Scheibe, T.D. (2020). Representing organic matter thermodynamics in biogeochemical reactions via substrate-

509 explicit modeling. *Frontiers in microbiology*, 11, p.531756. https://doi.org/10.3389/fmicb.2020.531756

510 Stegen, J.C., Johnson, T., Fredrickson, J.K. *et al.* (2018). Influences of organic carbon speciation on hyporheic

511 corridor biogeochemistry and microbial ecology. *Nat Commun* **9**, 585 https://doi.org/10.1038/s41467-018-02922-9

512 Stephanopoulos, George, Aristos A. Aristidou, and Jens Nielsen. (1998) Metabolic engineering: principles and

513 methodologies.

514 Tfaily, M. M., Chu, R. K., Toyoda, J., Tolić, N., Robinson, E. W., Paša-Tolić, L., & Hess, N. J. (2017). Sequential

515 extraction protocol for organic matter from soils and sediments using high resolution mass spectrometry. *Analytica*

516 *chimica acta*, 972, 54-61.

517 Tolic, N., Liu, Y., Liyu, A., Shen, Y., Tfaily, M. M., Kujawinski, E. B., ... & Hess, N. J. (2017). Formularity: software

518 for automated formula assignment of natural and other organic matter from ultrahigh-resolution mass spectra.

519 *Analytical chemistry*, 89(23), 12659-12665.

520 Wang, G., W.M. Post and M.A. Mayes (2013). Development of microbial-enzyme-mediated decomposition model

521 parameters through steady-state and dynamics analyses, *Ecological Applications*, 23(1), 255-272,

522 https://doi.org/10.1890/12-0681.1

523 Ward, N.D., Keil, R.G., Medeiros, P.M., Brito, D.C., Cunha, A.C., Dittmar, T., Yager, P.L., Krusche, A.V., Richey,

524 J.E. (2013) Degradation of terrestrially derived macromolecules in the Amazon River. Nature Geoscience. 6 (7), 530-

525 533. https://doi.org/10.1038/ngeo1817

526 Ward, N.D, Muller, K.A., Chen, X., Zhao, Q., Chu, R., Cheng, Z., Wietsma, T.W., Kukkadapu, R.K. (2023).

527 Interactive Effects of Salinity, Redox State, Soil type, and Colloidal Size Fractionation on Greenhouse Gas Production

528 in Coastal Wetland Soils. ESS Open Archive. https://doi.org/10.31223/X5FM0N